

Determination of the Coefficient of Diffusivity of Potential Vorticity in a Zonal Channel



Key Points:

- We develop an algebraic equation linking mean potential vorticity diffusivity coefficient with zonal velocity, wind, and bottom topography
- Numerical experiments reveal linear relationships between diffusivity and (a) wind stress and (b) a measure of the topographic gradient
- For realistic windstress, we found that eddy saturation is less likely to occur when topography is spatially smooth (low zonal wavenumber)

Correspondence to:

B. Sinha,
bs@noc.ac.uk

Citation:

Ivchenko, V. O., & Sinha, B. (2025). Determination of the coefficient of diffusivity of potential vorticity in a zonal channel. *Journal of Geophysical Research: Oceans*, 130, e2024JC021912. <https://doi.org/10.1029/2024JC021912>

Received 11 OCT 2024

Accepted 30 MAR 2025

Author Contributions:

Conceptualization: V. O. Ivchenko, B. Sinha

Formal analysis: V. O. Ivchenko, B. Sinha

Investigation: V. O. Ivchenko

Methodology: V. O. Ivchenko, B. Sinha

Validation: B. Sinha

Visualization: V. O. Ivchenko

Writing – original draft: V. O. Ivchenko

Writing – review & editing:

V. O. Ivchenko, B. Sinha

V. O. Ivchenko¹  and B. Sinha² 

¹University of Southampton, and National Oceanography Centre, Southampton, UK, ²National Oceanography Centre, Southampton, UK

Abstract Understanding mesoscale eddies and their interaction with the basin scale mean flow remains an important problem in physical oceanography. Several different approaches to parameterization of the effects of mesoscale eddies have been examined in the literature. In quasi-geostrophic potential vorticity (PV) transfer theory, mesoscale eddies are assumed on average to transfer PV downgradient and the main free parameter is the PV diffusivity coefficient, which is assumed to depend on the mean flow. Here, we adopt a new, complementary approach, which aims to develop strong constraints on the possible magnitude of the PV diffusivity due to parameters independent of the flow such as the wind stress and bottom topography. Combining results from an eddy resolving quasi-geostrophic model and a corresponding analytic model with parameterized eddies in a barotropic channel configuration, it is demonstrated that the PV diffusivity strongly varies for different types of bottom topography and for different wind stress with important consequences for the strength of the mean circulation. For monoscale (sinusoidal) topography, an algebraic equation is developed linking the PV diffusivity coefficient with the transport, wind stress, bottom topography, and geophysical and geometrical parameters. We present the result of statistical analysis of solutions of this equation with prescribed zonal transport obtained from a number of the eddy resolving model simulations and propose a new equation linking the PV diffusivity coefficient with wind stress and a parameter related to topographic roughness. We anticipate that similar relationships will hold for more realistic flow configurations and other types of mesoscale eddy closures.

Plain Language Summary The ocean is filled with eddies of quite small size (order 100 km) compared to the ocean basins. These so-called “mesoscale eddies” substantially influence the strength of the global ocean circulation including major currents such as the Atlantic Circumpolar Current in the Southern Ocean which in turn play a major role in maintaining Earth's climate. Here, we develop a mathematical approach which allows us to model the statistical effect of the eddies on the mean circulation without having to model every single eddy. Using this approach, we relate the impact of the mesoscale eddies on the circulation to the presence of bottom topography and the strength of the wind stress blowing over the ocean surface. The relationships we find can be used to better include the effects of mesoscale eddies in ocean and climate models.

1. Introduction

Numerical models of the oceanic circulation fall into two major classes, depending on size of the horizontal grid: fine resolution (FR) models and coarse resolution (CR) models. The former class includes models with a small enough horizontal grid to describe individual mesoscale eddies, and the latter class includes models with too coarse a grid to describe such eddies. The CR models require an eddy parameterization, which instead of modeling fields on the coarse grid approximates eddy effects in terms of mean properties of the model. Hence, new coefficients appear in the basic equations, which are generally speaking free parameters. Physical laws often impose limitations on these coefficients, but they cannot be specified as exact values/functions. As a result, numerical simulations with CR models depend on these coefficients. It is not obvious how to choose appropriate values of the coefficients and if there is a strong dependence of the circulation (i.e., values of the transport, energy, and geographical location of the main jets and gyres) on these coefficients an inappropriate choice could lead to unrealistic results. Developing a physically correct parameterization has both theoretical and practical value, leading to better understanding of the eddy-eddy, eddy-mean flow and eddy-topography interactions, and reducing computational expense. The latter reason is especially important in paleoceanography studies, where models are an indispensable tool due to a paucity of data (Wunsch (2003); Munday et al. (2013)) and because it is

© 2025. The Author(s).

This is an open access article under the terms of the [Creative Commons Attribution License](https://creativecommons.org/licenses/by/4.0/), which permits use, distribution and reproduction in any medium, provided the original work is properly cited.

too expensive for models simulating long periods of time to have a grid resolution fine enough to represent individual eddies.

Parameterizing the effect of mesoscale eddies using a diffusive parameterization of potential vorticity (PV) has a good physical basis. This parameterization was introduced by Green (1970) and Welander (1973) and developed in many studies, for example, Eden (2010), Eden and Greatbatch (2008), Ivchenko (1984), Ivchenko et al. (1997), Ivchenko et al. (2013), Killworth (1997), Marshall (1981), Marshall and Adcroft (2010), Marshall et al. (2012), Olbers et al. (2000), Ringler and Gent (2011), Treguier et al. (1997), Wardle and Marshall (2000), Ivchenko, Danilov, and Schroeter (2014), Ivchenko, Danilov, Sinha, and Schroeder (2014). A diffusive parameterization, that is, proportionality of eddy fluxes of any property to its mean gradient is applicable only for conserved properties, which excludes using this scheme for momentum but allows its use for PV.

The zonal channel could be seen as a simplified analog to the Antarctic Circumpolar Current (ACC). This simplification allows easy understanding of the dynamics of the zonal flow, which could be similar to the dynamics of the ACC. There is a well known strong dependence of the zonal transport of the ACC on the wind stress (Johnson and Bryden (1989); McWilliams et al. (1978); Munk and Palmen (1951); Wolff et al. (1991)). The response of the oceanic circulation to wind forcing is substantially different for models with high or low space resolution (Munday et al. (2013)). In a number of models, the zonal transport is much less sensitive to increasing wind stress using FR models than CR models (Constantinou and Hogg (2019); Hallberg and Gnanadesikan (2001); Munday et al. (2013); Tansley and Marshall (2001)). Because of the decisive role of mesoscale eddies, this reduced sensitivity is termed “eddy saturation.” Constantinou and Young (2017) studied the effect of random monoscale topography on forced β -plane turbulence using a one-layer quasi-geostrophic model. Special attention was paid to the regime of saturation. They find that baroclinic instability is not necessary for eddy saturation. One of the goals of the present paper is to revisit the problem of eddy saturation and investigate how it is affected by the presence of different types of topography.

Mesoscale eddies play a crucial role in the ACC not only for eddy saturation but in setting the ACC transport. Eddies participate in vertical transfer of the zonal momentum, which is imparted from the prevailing eastward wind stress at the surface down to the bottom (Ivchenko et al. (1996); Johnson and Bryden (1989); Marshall et al. (1993); Stevens and Ivchenko (1997)). Eddies also participate in reorganizing the zonal momentum, for example, increasing/decreasing momentum in the cores of zonal jets (Ivchenko (1984); Ivchenko et al. (1997), Ivchenko, Danilov, and Schroeter (2014); McWilliams et al. (1978); Treguier and McWilliams (1990); Wolff et al. (1991)) and sharpening of zonal flows by PV diffusion (Dritschel and McIntyre (2008); Wood and McIntyre (2010)).

In a number of studies with eddy parameterization, the coefficients are not physically motivated. Ivchenko et al. (2018) (hereinafter IZS) demonstrated a link between total zonal transport and the eddy PV diffusion coefficient (k_0). They showed that there is a huge range of zonal transport, corresponding to the smallest (i.e., $k_0 = 0$) and largest values of k_0 . Choosing an incorrect value of this coefficient leads to unrealistic ACC transport and the whole dynamics of the zonal channel. In the literature, the PV diffusivity coefficient has been assumed to depend on the mean flow (Green (1970); Held (1975); Killworth (1997); Marshall (1981)).

Here, we adopt a new, complementary approach, which aims to develop strong constraints on the possible magnitude of the PV diffusivity due to parameters independent of the flow such as the wind stress and bottom topography (and clearly this does not preclude additional flow-dependent variation). In view of the difficulty of diagnosing k_0 directly from eddy resolving models in the presence of bottom topography, we propose a novel way of choosing the coefficient of eddy potential diffusivity by matching values of the transport from numerical experiments with a FR finite difference model with those from a CR spectral-analytic model. The CR model employs a mesoscale eddy parameterization based on PV diffusion with truncated meridional wavenumbers but retains all the zonal wave numbers similar to Charney et al. (1981) and IZS. We develop a new equation, which links the coefficient k_0 with other parameters, both external (windstress) and internal (geometrical and geophysical). This is an algebraic cubic equation in k_0 . As a result of statistical analysis of the FR experiments, a new equation for k_0 as a function of wind stress and topographic roughness is presented.

The remainder of this paper is organized as follows. In Section 2, the basic equations of quasi-geostrophic barotropic zonal channel flow including eddy parameterization are introduced. The FR model and the CR model are formulated. A novel analytical expression for the coefficient of PV diffusivity is introduced. Section 3

presents the results of numerical experiments with the FR and the CR models. Section 4 compares the results of experiments with the Fine and the CR models. Section 4 also demonstrates the links between coefficient of PV diffusivity and the zonal transport. As a result of statistical analysis, a new equation for the coefficient of PV diffusivity as a function of wind stress and topographic roughness is presented. Section 5 consists of discussion and conclusions.

2. Basic Equations

2.1. Quasi-Geostrophic Equations for Barotropic Flow

The equation for barotropic quasi-geostrophic potential vorticity (QGPV) can be written as

$$\frac{\partial q}{\partial t} + J(\Psi, q) = T + F_B + F_H, \quad (1)$$

where q and Ψ are QGPV and streamfunction, respectively. Horizontal velocity $\mathbf{v} = (u, v)$ is related to the streamfunction by $u = -\frac{\partial \Psi}{\partial y}$ and $v = \frac{\partial \Psi}{\partial x}$, where u and v are the velocity components in the zonal (x) and meridional (y) directions. $J(A, C)$ is the Jacobian operator: $J(A, C) = -\frac{\partial A}{\partial y} \frac{\partial C}{\partial x} + \frac{\partial A}{\partial x} \frac{\partial C}{\partial y}$. T , F_B and F_H are the external forcing (wind stress), bottom, and horizontal friction, respectively.

The QGPV, q in barotropic flow represents the sum of relative vorticity, planetary vorticity, and the topographic term given by

$$q = \nabla^2 \Psi + f + \frac{f_0}{H} B, \quad (2)$$

where Coriolis parameter $f = f_0 + \beta y$. f_0 and β denote its value at a reference latitude and its meridional gradient, respectively. B is the deviation of bottom topography from a constant depth H .

2.2. The Fine Resolution (FR) Model

The FR model used herein is based on the quasi-geostrophic channel model described by Sinha and Richards (1999) run in barotropic mode and is an eddy-resolving model. It solves the barotropic quasi-geostrophic Equations 1 and 2 presented in Section 2.1 above in a zonally oriented reentrant (periodic) channel of length L_x , width L with rigid boundaries, that is, no normal flow boundary conditions to the north and south. The model is forced by a zonal wind stress in the traditional manner:

$$T = \frac{1}{H\rho_0} \text{curl}_z \boldsymbol{\tau}, \quad (3)$$

where $\boldsymbol{\tau}$ represents tangential wind stress, and ρ_0 is the water reference density,

$$\tau_x = \tau_0 \sin(\pi y/L), \quad (4)$$

$$\tau_y = 0. \quad (5)$$

Bottom friction has a linear friction law with coefficient ϵ

$$F_B = -\epsilon \text{curl}_z \mathbf{v}, \quad (6)$$

both identical to the CR model (Section 3.1 below). Unlike the CR model, lateral friction must be included for numerical stability and we specify a biharmonic lateral friction operator

$$F_H = A_6 \nabla^6 \Psi, \quad (7)$$

where A_6 is the friction coefficient.

A_6 is set to $1 \cdot 10^{10} \text{m}^4/\text{s}$ and all other parameters of the model are made identical to those chosen for the CR model (Section 3 below). The FR model Equations 1–7 were discretized for numerical solution using standard second-order centered differences in space on an Arakawa-C-type grid (Arakawa (1966)). Nonlinear terms were formulated using an energy and enstrophy conserving Jacobian (Arakawa and Lamb (1977)). In time, a leapfrog scheme was employed with an occasional forward time step to avoid development of a computational mode (Richtmyer and Morton (1967)). The time step was 1.5 hr and the horizontal resolution was chosen to be 10 km. In each of the experiments, the model was initialized from a state of rest. The bottom topography $B(x, y)$ is prescribed as depending sinusoidally on the y -coordinate with zero values on the walls ($y = 0$ and $y = L$)

$$B(x, y) = h(x) \sin\left(\frac{\pi y}{L}\right). \quad (8)$$

The zonal variation of the bottom topography is prescribed as a Fourier expansion

$$h(x) = \sum_n c_n \cos\left(\frac{2n\pi x}{L_x}\right) + \sum_n d_n \sin\left(\frac{2n\pi x}{L_x}\right), \quad (9)$$

where c_n and d_n are the amplitudes of the prescribed topography. n is the index of each mode used in the Fourier expansion.

2.3. The Coarse Resolution (CR) Model

In the CR models, individual mesoscale eddies are excluded, and since their influence on the mean flow is substantial, they (eddies) must be parameterized. The traditional diffusive parameterization of QGPV can be written as

$$\overline{\mathbf{v}'q'} = -k\nabla\overline{q}, \quad (10)$$

where k is the coefficient of eddy diffusivity of QGPV, and the overbar denotes an average. We use a combined time and partial zonal average (see IZS). Note, that the partial zonal and time average is a more appropriate type of average for the zonal channel domain with a variable topography than a time-only average, since bottom topography being time independent cannot contribute to the eddy topographic form stress in the case of time average. Note, that the zonal transport in case of partial zonal and time average is equal to the zonal transport in case of time-only average in reentrant channel. The CR model used in this study is a spectral-analytic model with parameterized eddies, according to (10) but otherwise having the same wind forcing, bottom topography, domain geometry, and geophysical parameters as the FR model. The diffusive parameterization can be applied only for conserved quantities, such as QGPV, but not for momentum, which is not conserved because of the pressure gradient force (Killworth (1997); Marshall (1981); Welander (1973)).

The coefficient k to be determined from 10 consists of divergent and rotational (dynamically nonactive) components. The decomposition of an eddy flux of PV into a divergent flux component and a rotational flux component is not unique in a bounded or periodic zonal channel domain (Fox-Kemper et al. (2003)). Therefore, we cannot specify k for the CR model simply by diagnosing it directly from the FR model. Instead, we use an alternative approach set out below.

We specify QGPV input due to surface wind stress and bottom friction exactly the same as it is for the FR model (3–5). Horizontal friction is disregarded.

The averaged Equation 1, using 10, becomes:

$$\overline{u} \frac{\partial \overline{q}}{\partial x} + \overline{v} \frac{\partial \overline{q}}{\partial y} - \frac{\partial}{\partial x} k \frac{\partial \overline{q}}{\partial x} - \frac{\partial}{\partial y} k \frac{\partial \overline{q}}{\partial y} = \frac{1}{H\rho_0} \text{curl}_z \overline{\boldsymbol{\tau}} - \epsilon \text{curl}_z \overline{\mathbf{v}}. \quad (11)$$

We specify the coefficient k to be constant and equal to the mean coefficient k_0 in most of the channel away from very thin boundary layers near the solid walls, where k exponentially reduces to zero. This distribution allows us to satisfy boundary conditions of no flux of QGPV through the solid walls (see IZS and Appendix A).

Charney et al., 1981 used zero boundary conditions for the mean zonal velocity U (i.e., $U = 0$ if $y = 0, L$) for the atmospheric zonal channel. For an oceanic zonal channel, where the main forcing is a wind stress Marshall (1981) demonstrated that mean zonally averaged velocity on the boundaries vanishes, if wind stress vanishes and if this velocity is zero initially. IZS used this boundary condition. However note, there is a jump in U if a zero boundary condition is imposed. This causes a problem because in order to solve Equation 11 we must integrate U and $\partial U/\partial y$ with respect to y , which is not possible if U is not smooth and differentiable (see Appendix B). To avoid this complication, we suggest the following way to use continuous and differentiable U^* , that is,

$$U^* = U\{1 + e^{(-L/\Delta)} - e^{(-y/\Delta)} - e^{(y-L)/\Delta}\}, \quad (12)$$

where Δ is the width of thin boundary layers, $\Delta \ll L$, and U is a constant. U^* is almost constant in the domain but quickly drops to zero on the side walls. The difference between U^* and U at any point of the domain will be small by choosing Δ to be small enough except on the solid boundaries, where $U^* = 0$. (see details on Appendix B).

We now assume that the solution for Equation 11 consists of a zonal flow with (unknown) velocity U^* and additional velocity linked with streamfunction Φ multiplied by the first meridional Fourier mode:

$$\bar{\Psi}(x, y) = -U(1 + e^{-L/\Delta})y - U\Delta e^{-y/\Delta} + U\Delta e^{(y-L)/\Delta} + \Phi(x) \sin\left(\frac{\pi y}{L}\right). \quad (13)$$

We follow Charney et al. (1981) who used a similar technique for an atmospheric flow in a zonal channel. We represent the topographic term B in the form 8. The net zonal transport across the channel depends only on U^* (with high accuracy on U), because $\Phi(x) \sin\left(\frac{\pi y}{L}\right)$ does not affect the net transport, although it does affect the zonal velocity locally because of topography and diffusion of the QGPV. We specify the surface wind stress $\bar{\tau} = (\tau_x, \tau_y)$ the same as in the FR model, that is, by Equations 4 and 5.

To obtain an analytical solution let us write Φ as Fourier series:

$$\Phi(x) = \sum_n a_n \cos\left(\frac{2n\pi x}{L_x}\right) + \sum_n b_n \sin\left(\frac{2n\pi x}{L_x}\right), \quad (14)$$

where a_n and b_n are unknown constants. (Recall n is the index of each mode used in the Fourier expansion.) The topographic term is written as in 9.

Using the technique developed by Charney et al. (1981) and applied by IZS (see Appendix B), after transformation one can write down $2n+1$ equations for $2n+1$ variables, that is, Fourier coefficients a_n, b_n and mean zonal velocity U .

$$-\left\{\frac{k_0(2n\pi)^2}{L_x^2} + \frac{k_0\pi^2}{L^2} + \epsilon + \frac{\epsilon L_x^2}{L^2 4n^2}\right\} a_n + \left\{\frac{\beta L_x}{2n\pi} - \frac{2n\pi U}{L_x}\right\} b_n + \frac{f_0 d_n L_x U}{H 2n\pi} + \frac{k_0 f_0 c_n}{H} = 0, \quad (15)$$

$$\left\{\frac{\beta L_x}{2n\pi} - \frac{2n\pi U}{L_x}\right\} a_n + \left\{\frac{k_0(2n\pi)^2}{L_x^2} + \frac{k_0\pi^2}{L^2} + \epsilon + \frac{\epsilon L_x^2}{L^2 4n^2}\right\} b_n + \frac{f_0 c_n L_x U}{H 2n\pi} - \frac{k_0 f_0 d_n}{H} = 0, \quad (16)$$

$$\frac{\pi}{4H\rho_0} \tau_0 - \frac{2f_0\pi}{3L_x H} \sum_n n(d_n a_n - c_n b_n) - \epsilon U - \frac{3\pi^2 k_0}{4L^2} U - k_0 \beta = 0. \quad (17)$$

If the topographic modes c_n and d_n are zero, then Equations 15 and 16 are homogeneous linear equations with respect to variables a_n and b_n and the solution of this system is $a_n = b_n = 0$. Only the Fourier modes represented in the bottom topography contribute.

For a prescribed zonal velocity U , Equations 15 and 16 can be reformulated to

$$a_n \left(k_0 A_2^{(n)} + A_3^{(n)}\right) + b_n A_1^{(n)} = c_n k_0 A_5^{(n)} + d_n A_4^{(n)}, \quad (18)$$

$$a_n A_1^{(n)} + b_n (-k_0 A_2^{(n)} - A_3^{(n)}) = -k_0 d_n A_5^{(n)} + c_n A_4^{(n)}, \quad (19)$$

where

$$A_1^{(n)} = \frac{U2n\pi}{L_x} - \frac{\beta L_x}{2n\pi}, \quad (20)$$

$$A_2^{(n)} = \frac{4n^2\pi^2}{L_x^2} + \frac{\pi^2}{L^2}, \quad (21)$$

$$A_3^{(n)} = \epsilon + \frac{\epsilon L_x^2}{L^2 4n^2}, \quad (22)$$

$$A_4^{(n)} = \frac{U f_0 L_x}{H 2n\pi}, \quad (23)$$

$$A_5^{(n)} = \frac{f_0}{H}. \quad (24)$$

These coefficients depend on the geometry of the channel (i.e., L_x , L and H), geophysical parameters f_0 , β , ϵ , and zonal transport (velocity U) but are independent of k_0 and wind stress τ_0 . Since we are looking only for eastward wind stress ($\tau_0 > 0$), the value of U must be positive.

The mean streamfunction is calculated using the CR model for all types of topography and for different amplitudes of the wind stress and for different values of k_0 . For any prescribed topography and wind stress, the zonal transport is a function of k_0 .

The zonal momentum contribution by wind is balanced by topographic form stress, bottom friction, friction due to PV diffusivity and by topographic form stress exerted by parameterized eddies (IZS). Therefore, the 5-th term on the R.H.S. of 17 should be less than or equal to the 1-st term on the R.H.S. (i.e., the wind stress), which yields the limitation of k_0 :

$$k_0 \leq k_M = \frac{\pi\tau_0}{4\beta H\rho_0}. \quad (25)$$

Note, that the actual maximum value of $k_0 = k_{\max}$ which corresponds to the zero value of transport is less than k_M , indeed:

$$k_{\max} < k_M. \quad (26)$$

The values of the transport occupy a range between the highest possible value, which corresponds to the zero value of the coefficient k_0 and zero-transport, which corresponds to the highest value of $k_0 = k_{\max}$. k_{\max} depends not only on wind stress, geometrical and geophysical parameters but also on the amplitude and spatial variability of topographic obstacles, that is, on zonal topographic Fourier number n . The spatial variability of topography may cause a stronger effect of the drag of the mean flow by the topographic form stress, bottom friction, friction due to PV diffusivity and by topographic form stress exerted by parameterized eddies. This reduces the transport, diminishing k_{\max} .

We require that only one value of k_0 is correct and the others are not correct. To specify this correct value of k_0 , we diagnose the transport from the FR model simulation for the same channel and for the same external forcing. Then, we find the steady-state zonal transport and choose the value of k_0 using the diffusivity-transport relationship from the CR model. The method is similar to the use of emergent constraints in climate model projections.

It is straightforward to find the solution, a_n and b_n , of the system of $2n$ equations (Equations 18 and 19). In the case of a zonal channel with monoscale topography, we can develop an analytical solution. If these solutions are substituted into Equation 17 after some transformations, we can find an expression linking k_0 with τ_0 and U :

$$M_3 k_0^3 + M_2 k_0^2 + M_1 k_0 + M_0 = 0, \quad (27)$$

where

$$M_3 = 12HL_x\beta A_2^{(n)2} + 9A_2^{(n)2}HL_x\pi^2U/L^2, \quad (28)$$

$$M_2 = 24HL_x\beta A_2^{(n)}A_3^{(n)} - 3\tau_0\rho_0^{-1}\pi L_x A_2^{(n)2} + 12HL_x\epsilon UA_2^{(n)2} + 18HL_x\pi^2UA_2^{(n)}A_3^{(n)}/L^2, \quad (29)$$

$$M_1 = 8f_0\pi n(c_n^2 + d_n^2)\left(A_2^{(n)}A_4^{(n)} - A_1^{(n)}A_5^{(n)}\right) + 12HL_x\beta\left(A_1^{(n)2} + A_3^{(n)2}\right) - 6\tau_0\rho_0^{-1}\pi L_x A_2^{(n)}A_3^{(n)} \\ + 24HL_x\epsilon UA_2^{(n)}A_3^{(n)} + \left(A_1^{(n)2} + A_3^{(n)2}\right)9\pi^2UHL_x/L^2, \quad (30)$$

$$M_0 = 8f_0\pi n(c_n^2 + d_n^2)A_3^{(n)}A_4^{(n)} - 3\tau_0\rho_0^{-1}\pi L_x\left(A_1^{(n)2} + A_3^{(n)2}\right) + 12HL_x\epsilon U\left(A_1^{(n)2} + A_3^{(n)2}\right). \quad (31)$$

Equation 27 is a 3-rd order algebraic equation in k_0 and includes U . This equation allows us to calculate k_0 based on a prescribed value of transport, which is known from FR experiments, or to calculate transport using a prescribed value of the coefficient k_0 .

3. Numerical Experiments With the FR and CR Models

Numerical experiments were run using both the FR model and the CR model. Standard geometrical and geophysical parameters relevant to the Southern Ocean were used in all the experiments: channel length $L_x = 4 \cdot 10^6$ m, width $L = 10^6$ m; reference depth $5 \cdot 10^3$ m; Coriolis parameter $f_0 = -10^{-4}$ s⁻¹, $\beta = 1.4 \cdot 10^{-11}$ m⁻¹s⁻¹, $\rho_0 = 10^3$ kg/m³, $\epsilon = 10^{-7}$ s⁻¹.

We studied a number of cases with different bottom topography (i.e., amplitudes of topography c_n , d_n and Fourier mode n). In our study, we concentrate on the monoscale type of topography with an amplitude between 100 and 300 m and Fourier modes between 1 and 7. The wind stress in these experiments is in the realistic range, varying between 0.1 N/m² and 0.3 N/m².

We used 100, 200, and 400 years of integration of the FR model and found that the time-averaged transport was not sensitive to the increasing time average. The experiments have demonstrated that equilibrium is achieved not later than 20 model years. Therefore, we used integration between 20 and 100 years as the standard integration time, and subsequent references to “transport” refer to the average transport over 80 model years.

Figure 1 (top and the 3-rd panels) displays time-mean streamfunctions calculated by the FR model for channels with topography represented by $c_2 = 300$ m for $\tau_0 = 0.1$ N/m², and $\tau_0 = 0.3$ N/m². The topography is presented in the bottom panel.

The flow strongly correlates with the topography and transport increases with increasing wind stress.

Equation 17 has a clear physical interpretation: the external and the only source term—the wind stress (the 1-st term) is balanced by four terms: by bottom form stress (the 2-nd term), by classic viscous bottom friction (the 3-rd term), by friction due to PV diffusivity (the 4-th term) and by the topographic form stress exerted by parameterized eddies (IZS) (the 5-th term). In most cases, the main balance takes place due to topographic form stress. This contribution reaches 93% of the wind forcing at $c_7 = 300$ m, $\tau_0 = 0.3$ N/m². The exceptions are the channels with small amplitude, smooth topography, when bottom friction ϵU or/and βk_0 terms becomes important. The contribution of a bottom friction can reach up to 70% ($c_1 = 100$ m), and contribution of βk_0 can reach up to 38%–39% ($c_1 = 100$ m, $c_3 = 100$ m, $c_2 = 200$ m). The contribution by PV-diffusivity ($3\pi^2 k_0 U / (4L^2)$) is negligible (no more than 4% at $c_1 = 200$ m, $\tau_0 = 0.3$ N/m²), in most cases nor more than 1%–2%.

The transport reduces if topographic Fourier mode n increases (when the amplitudes of the wind stress τ_0 and of the bottom topography are unchanged) (Figure 2).

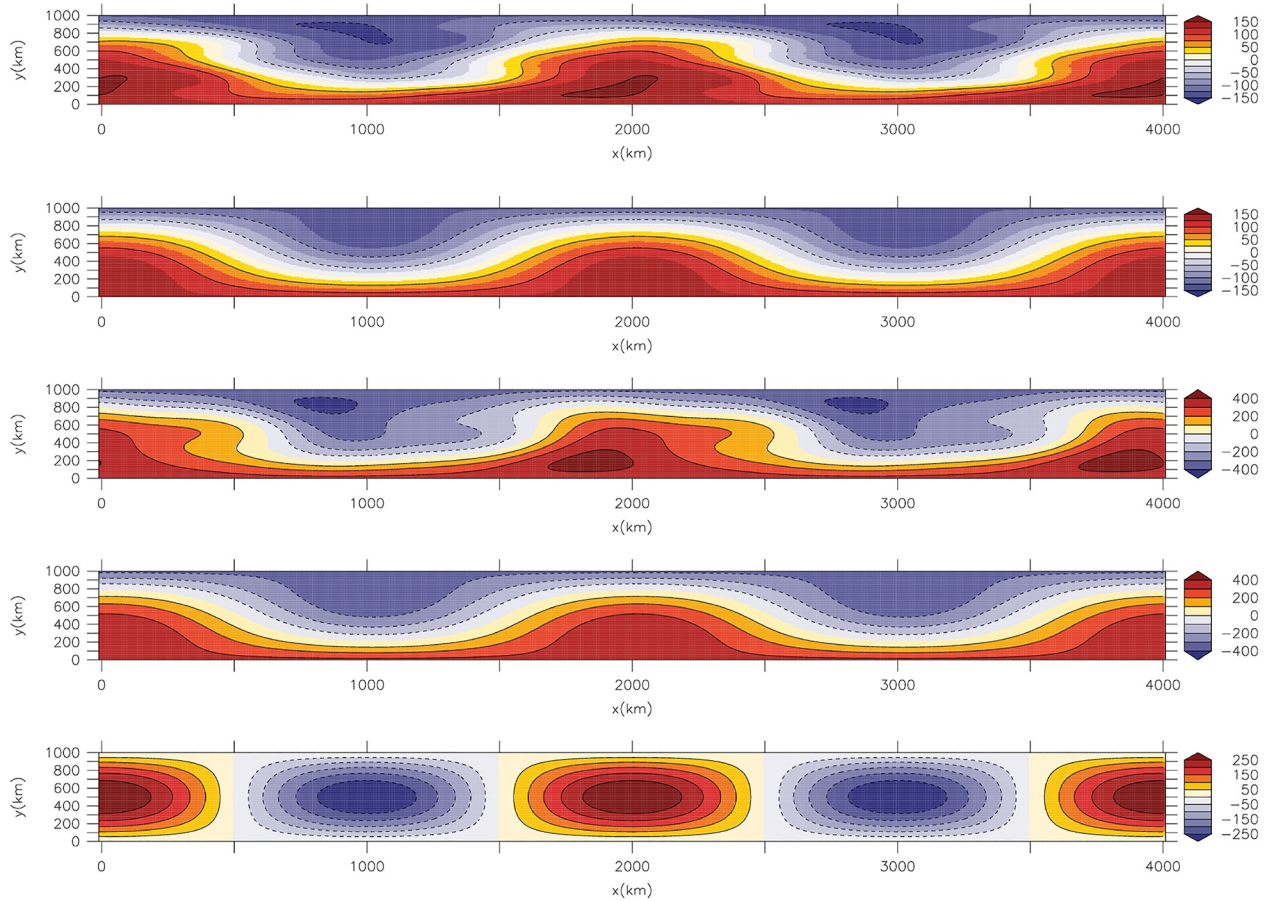


Figure 1. The averaged streamfunction times reference depth (Sv.) from the Fine Resolution (FR) model (top and 3-rd panels) and the averaged streamfunction times reference depth (Sv.) from the Coarse Resolution (CR) model (2-nd and 4-th panels). Topography represented by $c_2 = 300\text{m}$ (5-th panel). The wind stress is $\tau_0 = 0.1\text{ N/m}^2$ (1-st and 2-nd panels) and $\tau_0 = 0.3\text{ N/m}^2$ (3-rd and 4-th panels).

This can be explained by increasing topographic form stress. Increasing wind stress results in an increase of the transport (Figure 2). For example, the zonal transport for topography $c_1 = 100\text{ m}$ reaches 544.5 Sv. and 1,654.9 Sv. for wind stress $\tau_0 = 0.1\text{ N/m}^2$ and $\tau_0 = 0.3\text{ N/m}^2$, respectively. For topography $c_7 = 100\text{ m}$ the transport is reduced to 186.6 Sv. and 274.2 Sv. for wind stress $\tau_0 = 0.1\text{ N/m}^2$ and $\tau_0 = 0.3\text{ N/m}^2$, respectively. The transports for topography $c_1 = 300\text{ m}$ are 338.5 and 668.5 Sv. for wind stress $\tau_0 = 0.1$ and 0.3 N/m^2 , respectively. For topography $c_7 = 300\text{ m}$ the transports drop to 70.3 Sv. and 119.4 Sv, for wind stress $\tau_0 = 0.1$ and 0.3 N/m^2 , respectively (Figure 2).

Because we have a large number of numerical experiments with different wind stress applied to the FR model it is straightforward to see whether eddy saturation takes place. For high topographic Fourier number ($n > 4$) there is definitely an eddy saturation regime (see Figure 2). For example, for $c_6 = 300\text{ m}$ transport increases from 141.2 Sv. to 156.1 Sv. for $\tau_0 = 0.2\text{ N/m}^2$ and $\tau_0 = 0.3\text{ N/m}^2$, respectively. In contrast, in the case of topography $c_1 = 200\text{ m}$ there is no saturation: transport increases from 430.8 Sv. ($\tau_0 = 0.1\text{ N/m}^2$) to 657.2 Sv. ($\tau_0 = 0.2\text{ N/m}^2$) and to 1,064.3 Sv. ($\tau_0 = 0.3\text{ N/m}^2$). Similarly for $c_1 = 100\text{ m}$ transport increases from 1,036.2 Sv. (when $\tau_0 = 0.2\text{ N/m}^2$). to 1,654.9 Sv. ($\tau_0 = 0.3\text{ N/m}^2$) and for $c_3 = 100\text{ m}$ transport increases from 575.5 Sv. ($\tau_0 = 0.2\text{ N/m}^2$) to 906.5 Sv. ($\tau_0 = 0.3\text{ N/m}^2$). We suggest that the lack of saturation in channels with small amplitude, smooth topography is due to fact that in this case an important role in the momentum balance is played by bottom friction (term ϵU in 17). The increase in windstress should lead to an increase in the mean zonal velocity U for balance, and accordingly, to the lack of saturation. There are a few intermediate cases with topography with amplitude of 200 m and topographic Fourier numbers 2–4 where

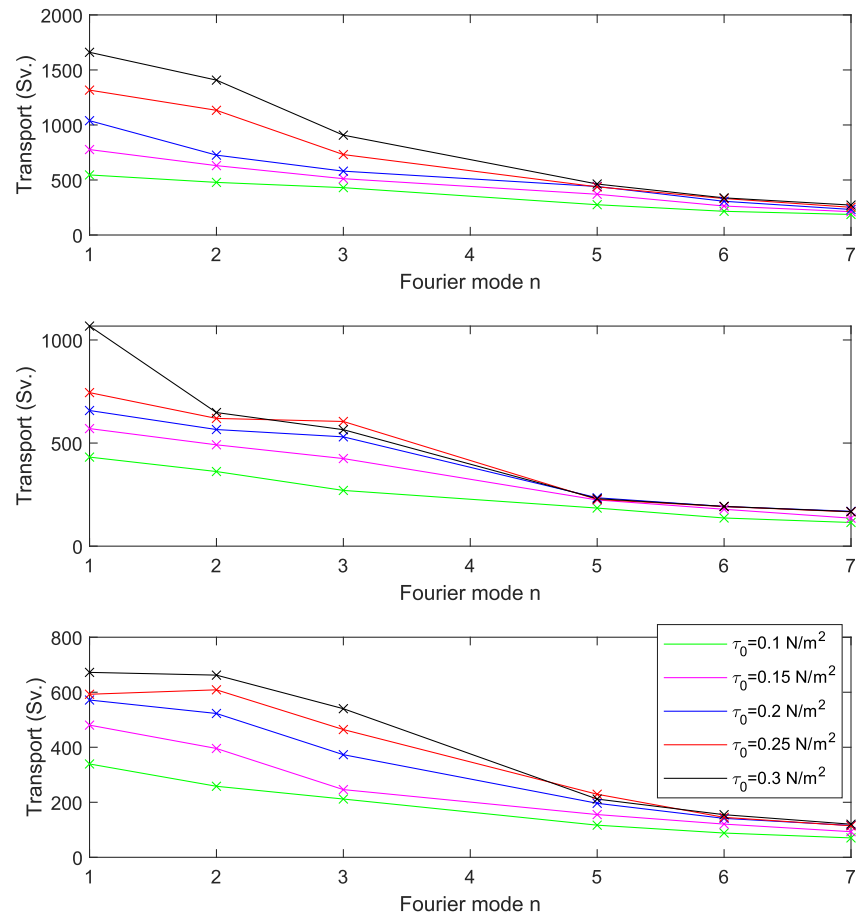


Figure 2. Zonal transport (Sv.) from FR model as a function of topographic Fourier modes for different wind stress. Topographic amplitude is 100 m (top panel), 200 m (middle panel), 300 m (lower panel).

saturation seems to occur at the higher end of the windstress range ($\tau_0 = 0.2 - 0.3 \text{ N/m}^2$) seen in the middle panel of Figure 2.

4. Comparison of Results From CR and FR Models and Developing Equations for k_0

Both the FR and the CR models simulate eastward flows (for eastward wind stress) strongly influenced by bottom topography (see Figure 1). The figure compares streamfunctions for channel flow with topography represented by $c_2 = 300 \text{ m}$ from the FR model (the top and the 3-d panel) and the CR model (the 2-nd and the 4-th panels) for $\tau_0 = 0.1 \text{ N/m}^2$, $\tau_0 = 0.3 \text{ N/m}^2$. The topography is presented in the bottom panel. Diffusivity coefficient $k_0 = 165.1 \text{ m}^2/\text{s}$ is used for the CR experiment with $\tau_0 = 0.1 \text{ N/m}^2$ and $k_0 = 572.9 \text{ m}^2/\text{s}$ for $\tau_0 = 0.3 \text{ N/m}^2$. These choices of k_0 give zonal transports in the CR model equal to the transports obtained from the FR experiments, that is, 257.6 Sv. and 662.4 Sv. for $\tau_0 = 0.1 \text{ N/m}^2$ and $\tau_0 = 0.3 \text{ N/m}^2$, respectively. The flow strongly correlates with the topography and transport increases when wind stress increased. The structure (i.e., direction) of the mean flow looks similar for different values of wind stress, increasing wind stress results in increasing transport (Figure 2). Experiments with the FR model for a channel with the same topography and wind stress looks generally similar in direction and in the amplitude of velocity to experiments with the CR model (see Figure 1). The kinetic energy and the zonal transport in the FR model reach a steady-state value after a few years of integration from the rest and have temporal variability linked with eddies. For some types of topography and for not too high wind stress, the amplitude of the temporal variability is rather small. However, increasing wind stress for similar topography leads to much higher variability of energy and transport.

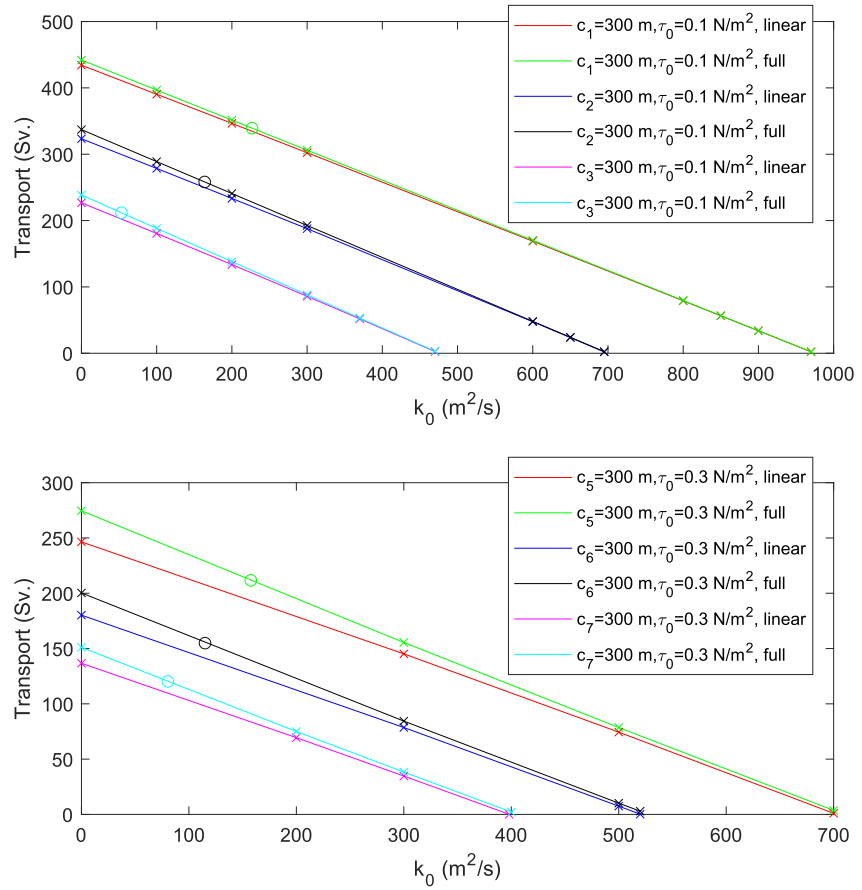


Figure 3. Zonal transport (Sv.) as a function of k_0 (as a solution of Equations 27 and 37) for three different topographic lengthscales. $\tau_0 = 0.1 \text{ N/m}^2$ (upper panel) and $\tau_0 = 0.3 \text{ N/m}^2$ (lower panel). Transports, which match the transport in the FR model and Equation 27, are marked by open circles.

We can see a linear decrease of the transport with increasing value of k_0 (see Figure 3). Increase of the number of the Fourier modes n leads to decreasing transport if τ_0 is fixed (see Figure 2), because of increasing of the bottom form stress.

4.1. Establishing a Relationship Between k_0 and Zonal Transport

For the range of the parameters expected, the cubic and quadratic terms of k_0 that is, $|M_3 k_0^3|$ and $|M_2 k_0^2|$ are several orders (at least two orders) of magnitude smaller than the terms of $|M_1 k_0|$ and $|M_0|$ and can be neglected. For most parameter values, the 3-rd, 4-th, and 5-th components of M_1 30, that is, $|6\tau_0\rho_0^{-1}\pi L_x A_2^{(n)} A_3^{(n)}|$, $|24HL_x \epsilon UA_2^{(n)} A_3^{(n)}|$, and $|((A_1^{(n)})^2 + A_3^{(n)2})9\pi^2 UHL_x/L^2|$ are usually much smaller than the 1-st and the 2-nd components of 30 that is, $|8f_0\pi n(c_n^2 + d_n^2)(A_2^{(n)} A_4^{(n)} - A_1^{(n)} A_5^{(n)}) + 12HL_x \beta(A_1^{(n)2} + A_3^{(n)2})|$. These components account for only a few percent of the 1-st and 2-nd components of M_1 . However, for the small and smooth topographic amplitudes (i.e., $c_1 = 100 \text{ m}$) and for strong wind ($\tau_0\rho_0^{-1} = 0.3 \text{ N/m}^2$), these three terms reach 18%. For explanation of the linear dependence between U (or transport) and k_0 , this accuracy is good enough to drop them out. Note that for our calculations of k_0 , we use a cubic Equation 27 without neglecting of any terms.

If we substitute (20–24) in Equation 27, we get Equation D1 (see Appendix D). The terms proportional to cubic and quadratic orders of U are also much smaller than the other terms and can be neglected (see Appendix D). Equation 27 after simplification can be rewritten in the form:

$$U = \frac{\tau_0 \rho_0^{-1} T_2^2 - k_0 T_4^2}{T_1^2 - k_0 T_3^2}, \quad (32)$$

where

$$T_1^2 = \frac{3HL_x^3 \epsilon \beta^2}{n^2 \pi^2} + 12H\epsilon^3 L_x + \frac{6HL_x^3 \epsilon^3}{L^2 n^2} + \frac{3HL_x^5 \epsilon^3}{4L^4 n^4} + 6\tau_0 \rho_0^{-1} L_x \pi \beta + (c_n^2 + d_n^2) \frac{4f_0^2 \epsilon L_x}{H} + (c_n^2 + d_n^2) \frac{f_0^2 \epsilon L_x^3}{H n^2 L^2}, \quad (33)$$

$$T_2^2 = \frac{3L_x^3 \beta^2}{4n^2 \pi} - 3\pi \epsilon^2 L_x + \frac{3\pi L_x^3 \epsilon^2}{2L^2 n^2} + \frac{3\pi L_x^5 \epsilon^2}{16L^4 n^4}, \quad (34)$$

$$T_3^2 = -(c_n^2 + d_n^2) L_x \frac{4f_0^2 \pi^2}{HL^2} + 24HL_x \beta^2, \quad (35)$$

$$T_4^2 = (c_n^2 + d_n^2) L_x \frac{4f_0^2 \beta}{H} + \frac{3HL_x^3 \beta^3}{n^2 \pi^2} + 12HL_x \beta \epsilon^2 + \frac{6H\beta \epsilon^2 L_x^3}{L^2 n^2} + \frac{3HL_x^5 \beta \epsilon^2}{4L^4 n^4}. \quad (36)$$

The only negative term in T_2^2 (see 34) is the 2nd term, that is, $-3\pi \epsilon^2 L_x$. The absolute value of this term is smaller than the value of the 1st term, that is, $\frac{3L_x^3 \beta^2}{4n^2 \pi}$ if $n < 89$, which confirms a positiveness of T_2^2 . The positiveness for the term T_3^2 is satisfied for topography lower than 545.8 m. The higher values of amplitude of the topographic obstacle cannot be applied because of the quasi-geostrophic limitations. In the range of parameters considered the second term in the denominator of 32 is much smaller than first one: usually it is a few percent of the 1st term; however in case of a strong windstress ($\tau_0 \rho_0^{-1} = 0.25$ N/m² and with small topographic amplitude of 100 m) it rose to 0.18. With the goal to simplify the expression (32) and to justify a linear relationship between U (transport) and k_0 , we can neglect the 2nd term in the denominator of this expression.

Equation 32 can be rewritten as

$$U = \tau_0 \rho_0^{-1} \frac{T_2^2}{T_1^2} - k_0 \frac{T_4^2}{T_1^2}. \quad (37)$$

There is a linear dependence of zonal velocity U (or zonal transport) on k_0 and this explains the linear relationship between U and k_0 in Figure 3, which was calculated from the basic equations. The maximum value of U corresponds to the zero value of k_0 and is a function of wind stress:

$$U_{\max} = \tau_0 \rho_0^{-1} \frac{T_2^2}{T_1^2}. \quad (38)$$

The maximum value of the k_0 is

$$k_{\max} = \tau_0 \rho_0^{-1} \frac{T_2^2}{T_4^2}. \quad (39)$$

It is interesting to compare k_{\max} from 39 with 25: in Figure 3 k_{\max} is indeed much smaller than k_M from 25. The difference in transports between FR experiments and CR experiments with $k_0 = 0$ (no parameterization) is substantial (see Figure 3). The difference could be between a few percent and more than 100%. For example, for topography $c_2 = 200$ m and wind stress of 0.3 N/m², the FR model gives transport of 649.9 Sv., and CR model with $k_0 = 0$ gives 1,305.8 Sv. Figures 4 and 5 demonstrate the dependence of k_0 on wind stress τ_0 and zonal Fourier mode in two different ways. For amplitude of topographic obstacle between 200 m and 300 m, Figure 4 plots k_0 as a function of Fourier mode for a number of different wind stress values, while Figure 5 plots k_0 as a

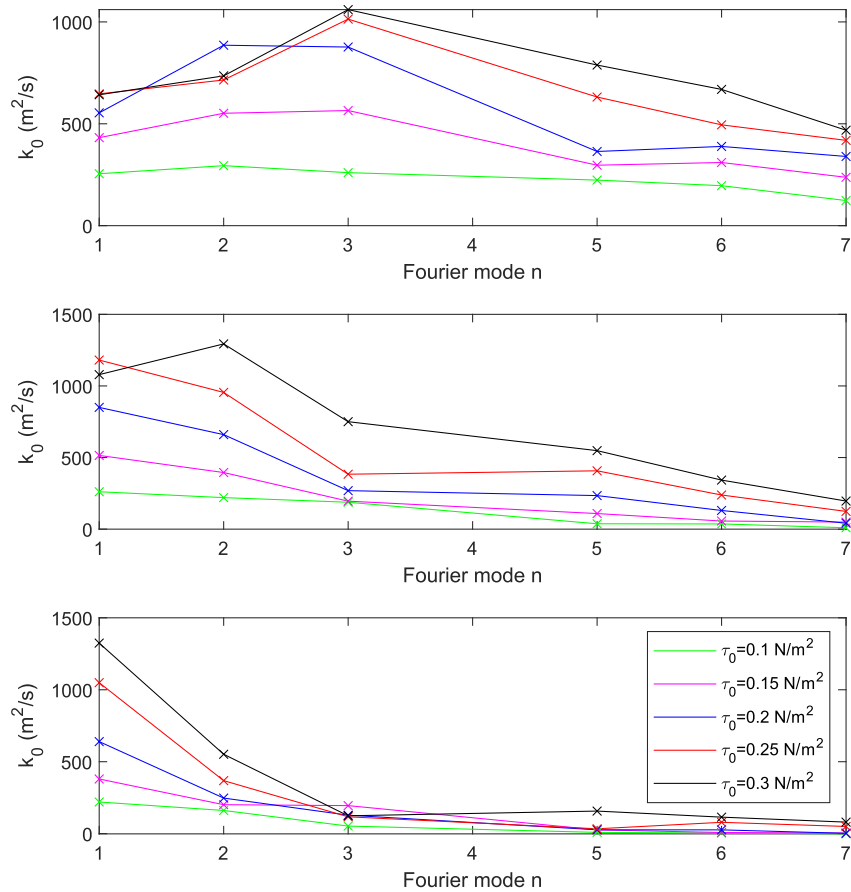


Figure 4. Dependence of k_0 on topographic Fourier modes. Topographic amplitudes 100 m (upper panel), 200 m (the second panel), and 300 m (lower panel). Colored lines show how the relationships vary with wind stress.

function of wind stress τ_0 for a single amplitude of topographic obstacle of 200 m for a number of different Fourier modes.

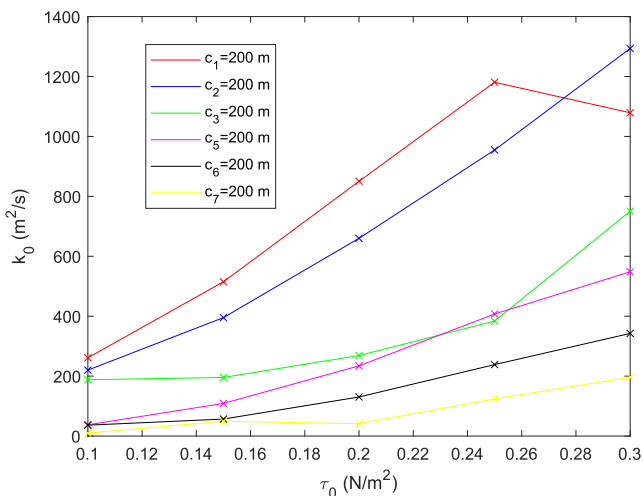


Figure 5. Coefficient k_0 for topographic amplitude of 200 m as a function of wind stress τ_0 .

Generally, the coefficient k_0 increases with increasing τ_0 . The values of k_0 reduce with increasing wave number with fixed wind stress.

In most cases, k_0 decreases for the same topography and wind stress when Fourier modes grow (see Figure 4). However, in the case of small amplitude topography ($c_n = 100$ m) and small Fourier modes ($n = 1-3$), the value of k_0 increases, when n increases. With small amplitudes and smooth (small n) topography, the main balance of windstress is viscous bottom friction (ϵU) together with the topographic form stress exerted by parameterized eddies (βk_0): $\tau_0 \pi / (4H\rho_0) \approx \epsilon U + \beta k_0$. For example, at $c_1 = 100$ m, the contribution of bottom friction is 70%, and the contribution of βk_0 is 23% ($\tau_0/\rho_0 = 0.1$ N/m²). Approximately the same balance remains even when the windstress increases to 0.2 N/m² (66% and 25%, respectively), and when the windstress increases to 0.3 N/m² (70% and 19%, respectively). We know that mean zonal velocity (transport) decreases with the growth of topographic Fourier mode n . Consequently, with the growth of n at a given windstress, the coefficient k_0 should increase for balance of windstress. Also, in the case of a large topographic amplitude ($c_n = 300$ m) and larger Fourier wavenumber, k_0 for $n = 6$ is more than k_0 for $n = 5$. k_0 more or less monotonically increases when wind stress increases for $c_n = 200$ m and $c_n = 300$ m, if

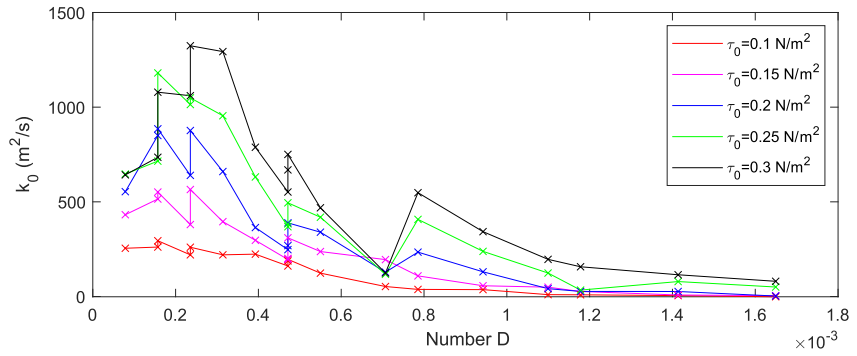


Figure 6. Coefficient k_0 as a function of D , which provides transport in the Coarse Resolution model equal to transport in the Fine Resolution model.

$n = 1, 2$ (Figure 4). However, there are some instances of nonmonotonic dependence of k_0 on the wind stress for $c_2 = 100$ m; for $c_n = 100$ m for $n = 5, 6$; for $c_n = 200$ m, $n = 1$). Equation 27 applies for monoscale topography. For multiscale topography, mathematical complications arise in deriving the equation, which links k_0 and τ_0 . However, it is straightforward to find the dependence numerically.

4.2. Derivation of an Equation for k_0 as a Function of Topographic Roughness and Wind Stress

Our results demonstrated a strong dependence of k_0 on topography, both on the amplitude of topography and the horizontal variability (topographic Fourier number). It would be interesting to introduce a topographic parameter combining both the amplitude and the horizontal variability with the aim of linking the coefficient k_0 with such a parameter. Recall that the important momentum sink of the external forcing (wind stress) in a zonal channel is the topographic form stress, which strongly depends on the zonal gradient of the topographic height. To quantify this dependence, an integral measure D of the roughness of the topography was introduced in IZS. The dimensionless number D is:

$$D = \sqrt{\frac{1}{LL_x} \int_0^L \int_0^{L_x} (\partial B / \partial x)^2 dx dy}. \quad (40)$$

This parameter D is the R.M.S. of the zonal gradient of B (recall that B is the deviation of bottom topography from a constant depth H). Substituting Equations 8 and 9 to 40 with an appropriate Fourier transformation, we obtain:

$$D = \frac{\pi}{L_x} \sqrt{\sum_n n^2 (c_n^2 + d_n^2)}. \quad (41)$$

The dependence of k_0 on D was calculated for wind stress τ_0 between $\tau_0 = 0.1$ and 0.3 N/m² and is shown in Figure 6.

For each value of τ_0 one can see the link between k_0 and D . The value of k_0 decreases when D increases. There is some nonmonotonic dependence of k_0 on D , such as the increase of k_0 in the interval of $D = 0.7 \cdot 10^{-3} - 0.8 \cdot 10^{-3}$ for wind stress between $\tau_0 = 0.2$ N/m² and $\tau_0 = 0.3$ N/m². This indicates the need for statistical analysis of the results. We fit these curves using linear regression. Figure 7 displays the linear fit for 5 values of the wind stress together with the 95% significance intervals. The absolute magnitudes of the correlation coefficients in Figure 7 are all >0.8 and significant with $>99\%$ confidence. These results confirm the possibility of representing k_0 as a linearly decreasing function of D as a first approximation.

To study the relationship between k_0 and τ_0 , we averaged k_0 over all values of D for each τ_0 (see Figure 8). The relationship k_0 - τ_0 is linear on the interval of τ_0 between 0.1 N/m² and 0.3 N/m².

We introduce a coefficient $k_0^0(\tau_0)$ representing a linear interpolation of k_0 corresponding to the minimum value of D (called D^0) between $\tau_0 = 0.1$ N/m² and $\tau_0 = 0.3$ N/m². $D^0 = 7.85 \cdot 10^{-5}$ corresponds to topography $c_1 = 100$ m. The equation linking k_0 with τ_0 and D can be written as follows:

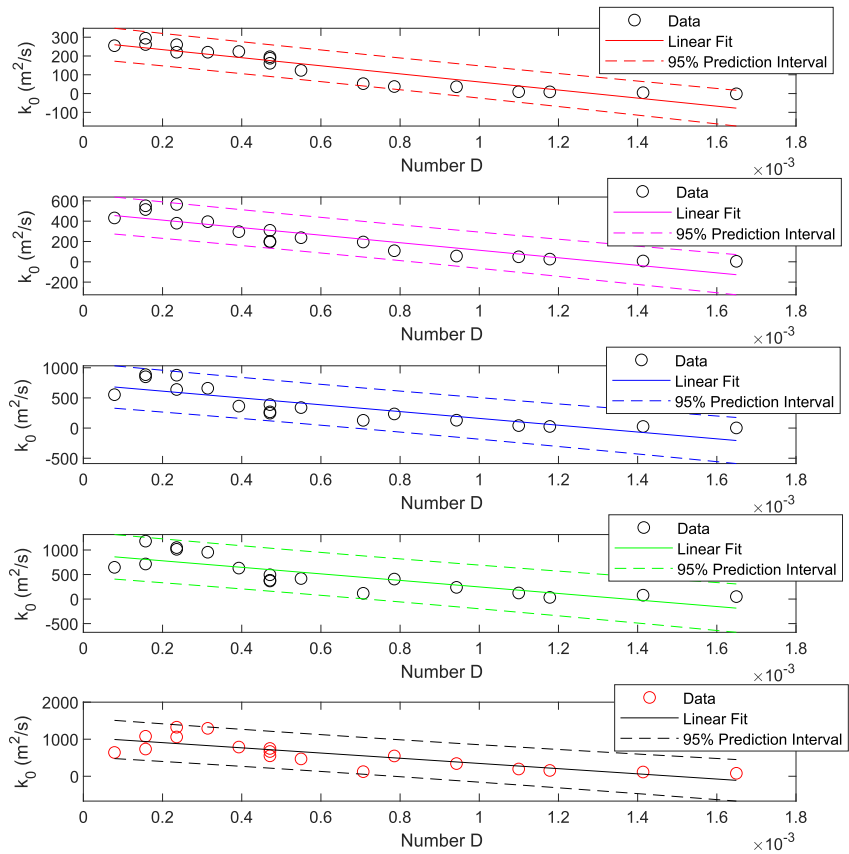


Figure 7. Linear fit of coefficient k_0 with 95% confidence interval; wind stress $\tau_0 = 0.1 \text{ N/m}^2$ (1-st panel), wind stress $\tau_0 = 0.15 \text{ N/m}^2$ (2-nd panel), wind stress $\tau_0 = 0.2 \text{ N/m}^2$ (3-rd panel), wind stress $\tau_0 = 0.25 \text{ N/m}^2$ (4-th panel), wind stress $\tau_0 = 0.3 \text{ N/m}^2$ (5-th panel). Correlation coefficients are -0.93 , -0.90 , -0.85 , -0.83 , and -0.81 , respectively, all significant with $>99\%$ confidence.

$$k_0(\tau_0, D) = k_0^0(\tau_0) + \alpha(D - D^0), \quad (42)$$

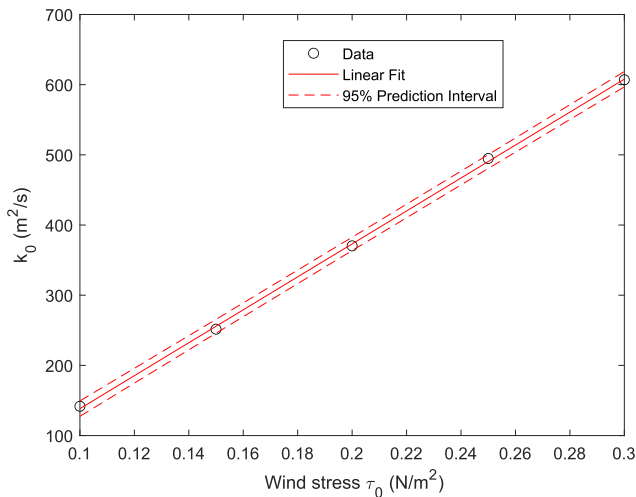


Figure 8. Dependence of mean k_0 on wind stress and linear fit with 95% confidence interval. Each data point is the result of average over 18 members. The correlation coefficient is 0.99 , significant with confidence $>99\%$.

where α is the average value of linear regression for $k_0(\tau_0, D)$ (see Figure 7). Parameter α generally depends on τ_0 , which can be seen from Figure 7: the slope of linear regression changes. To test this formula, 14 additional Control experiments with the FR model were performed. For our Control experiments, we have taken the α average. In these Control experiments, the wind stress and topography parameters were chosen randomly and differed from the parameters in the 90 experiments on which Figure 8 is based. The list of parameters for these 14 additional experiments is given in Appendix C. Figure 9 (upper panel) shows the comparison of diffusivity PV coefficients calculated using Equation 27 (i.e., based on the FR experiments and our theory) and Equation 42. The former coefficient we will call k_0^{FR} and the latter call k_0^{CR} . The parameters used for the calculation are shown in the lower panel of Figure 9.

The results confirm the validity of the proposed formula 42. k_0^{FR} and k_0^{CR} are significantly correlated with a correlation coefficient of 0.9 significant with $>99\%$ confidence. The distribution of k_0^{CR} is smoother than the distribution of k_0^{FR} . The values of k_0^{CR} in almost all control experiments are slightly less than that k_0^{FR} . The difference between the coefficients could be reduced by

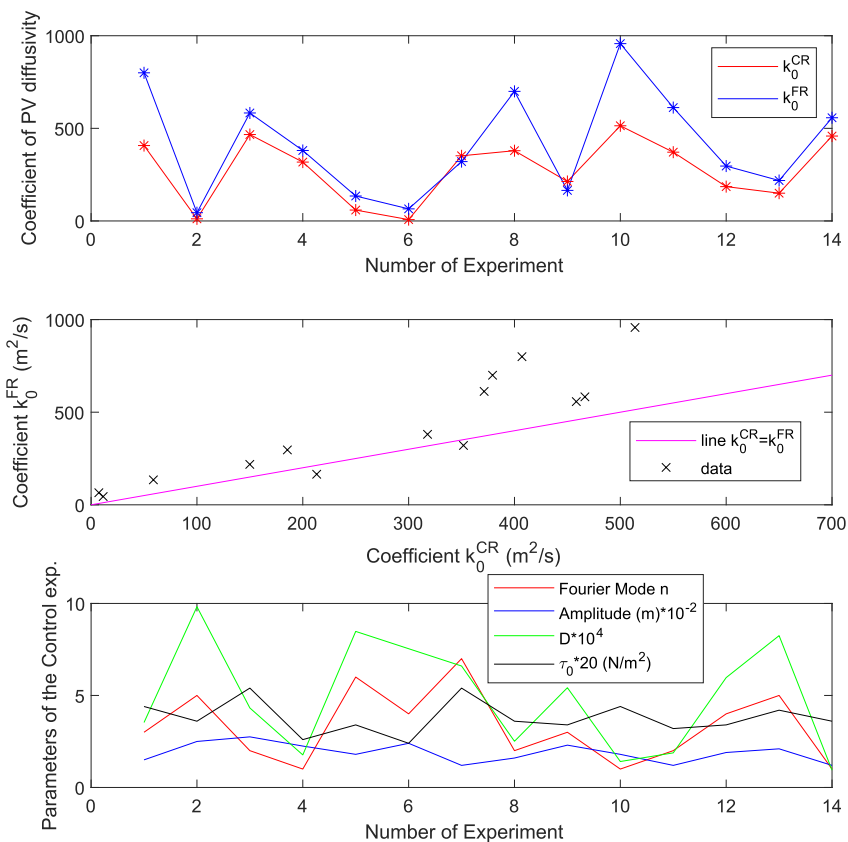


Figure 9. Coefficients k_0^{CR} and k_0^{FR} calculated for 14 additional Control experiments with random windstress and topography parameters (upper panel); scatter plot of the coefficients k_0^{FR} versus k_0^{CR} (middle panel); parameters, used in Control experiments to calculate k_0^{CR} (lower panel). The correlation coefficient between k_0^{CR} and k_0^{FR} is 0.9, significant with >99% confidence.

allowing the parameter α to be a function of wind stress. There is a linear dependence k_0^{FR} on D , but the regression coefficient generally depends on the wind stress (see Figure 7).

5. Discussion and Conclusions

All schemes of eddy parameterization contain coefficients, which are the “free parameters”, that is, parameters that cannot easily be specified from observations, theory, or eddy experiments. Any results providing us more information about the magnitude of these coefficients (e.g., k_0 in the diffusive PV parameterization), their space and time variability, or their dependence on windstress and on bottom topography are valuable. There are a few approaches that allow one to estimate or limit possible values of these coefficients. For example, integral constraints required the averaged coefficient k_0 to be positive (see IZS). Marshall (1981) demonstrated that in a two layer quasi-geostrophic zonal channel with a flat bottom, the coefficient of diffusivity of PV must be greater in the lower layer than in the upper layer. Contrary to the flat bottom case, the coefficient of diffusivity of PV in the upper layer must be greater than in lower layer, if the bottom topography deviation is high enough (Ivchenko et al. (2013)). Integral constraints required dependence of the coefficient of PV diffusivity on topography (Cummins (2000)).

The standard range of wind stress amplitude τ_0 between 0.1 N/m² and 0.3 N/m² was applied to all types of discussed topography. The contribution of wind stress in the zonal momentum equation is balanced by four terms (Equation 17): topographic (bottom) form stress, viscous bottom friction, friction due to PV diffusivity, and by the topographic form stress exerted by parameterized eddies βk_0 (IZS). In most cases, the main balance takes place due to topographic form stress, which is in agreement with the pioneering result of Munk and Palmen (1951) for the ACC and modeling results by Ivchenko et al. (1996) and Stevens and Ivchenko (1997). The exceptions are the

channels with small amplitude, smooth topography, when bottom friction ϵU or/and βk_0 terms becomes important. The contribution by PV-diffusivity ($3\pi^2 k_0 U / (4L^2)$) is negligible. The relative importance of the four balancing mechanisms depends on topography and wind stress amplitude.

Although many studies have assumed that the PV diffusion coefficient is a function of the mean flow, our study adopts a complementary approach and investigates whether factors which are independent of the mean flow such as the wind stress or the bottom topography can be used to constrain the diffusion coefficient.

We propose a new method for estimating the coefficient of diffusivity of PV based on a simplified model (CR) and using a number of the eddy resolving experiments (FR). The main results of this study are the derivation of two Equations 27 and 42. The former equation represents an analytical algebraic cubic equation, linking k_0 with the prescribed mean zonal velocity U (zonal transport) and wind stress τ_0 as well as geometric and geophysical parameters. This equation is developed for monoscale topography. Note, that this equation can be simplified to the linear Equation 37 by neglecting many relatively small terms. This equation demonstrates the range of values of k_0 (for each topography, and wind stress): the smallest $k_0 = 0$ which provides the highest value of the transport, and the maximum k_{\max} (expression 39) which provides zero zonal transport. The zonal transport strongly depends on the value of k_0 . Choosing an incorrect value of k_0 will lead to incorrect transport in a CR run.

Equation 42 is based on Equation 27, and on statistical analysis of ninety 100-model year eddy-resolving experiments (5 values of the wind stress applied to 3 values of the topographic amplitudes and 6 values of the Fourier modes). This analysis allows us to propose a linear relationship between k_0 and wind stress τ_0 and also a linear relationship between k_0 and a measure of topographic roughness, D (the R.M.S. of the zonal gradient of B).

To check the proposed parameterization, that is, Equation 42, a series of 14 additional experiments was performed using the FR model. In these experiments, wind stress and topography differed from the parameters of the original 90 experiments. The results showed a good match of parameterized k_0^{CR} and k_0^{FR} , that is, calculated using 27. Note that there are limitations for use of Equation 42, since the parameters of k_0^0 and α depend on the wind stress and they need initial experiments to determine them. Equation 42 is an empirical relationship between the diffusion and bottom roughness and wind stress.

Neglecting parameterization in the CR model, ($k_0 = 0$) yields substantial deviations from FR experiments: the difference is between a few percent and more than 100% (if $c_2 = 200$ m, and wind stress is 0.3 N/m^2). There are no truncation errors in the horizontal expansion, since only Fourier modes represented in the bottom topography contribute.

In this study, we revisited the problem of the eddy saturation. Many experiments with the FR model were conducted for various types of bottom topography. For most types of bottom topography, there is an eddy saturation regime. However, in channels with small amplitude and smooth topography, eddy saturation is not observed (see Figure 2). We suggest this lack of saturation is due to fact that in this case an important role in momentum balance is played by viscous bottom friction. The increase in windstress should lead to an increase in the mean zonal velocity for balance, and accordingly, to the lack of saturation.

A new important problem will be addressed in a future study: a generalization of this study to baroclinic zonal flows. The method proposed in this study can be generalized to the baroclinic two/three layer case. Mathematical complications will probably not allow us to develop an analytical equation similar to 27. However, numerical calculations will allow us to determine the vertical variability of coefficient of PV diffusivity as well as the thickness diffusion coefficient in the Gent-McWilliams scheme (Gent and McWilliams (1990)) based on the statistical analysis of the eddy-resolving models. Elucidating the dependence of these coefficients on wind stress and bottom topography would be a significant step in oceanic modeling.

Appendix A: Special Form of the Coefficient k_0

We assume no mass flux through the solid walls:

$$\bar{v}|_{y=0,L} = 0. \quad (\text{A1})$$

We also assume no QGPV flux through the walls:

$$\overline{v'q'}|_{y=0,L} = -\left(k \frac{\partial \bar{q}}{\partial y}\right)|_{y=0,L} = 0. \quad (\text{A2})$$

Condition A2 can only be satisfied if k is zero on the solid walls, because of the presence of the planetary vorticity gradient β in the expression for the meridional gradient of QGPV, that is, on the boundaries $\frac{\partial \bar{q}}{\partial y}$ cannot be zero; therefore, k must be zero. Hence, we specify the following form of the coefficient k :

$$k = k_0 \{1 + e^{(-L/\Delta)} - e^{(-y/\Delta)} - e^{(y-L)/\Delta}\}, \quad (\text{A3})$$

where Δ is the width of thin boundary layers, $\Delta \ll L$, and k_0 is a constant.

k is almost constant in the domain but quickly drops to zero on the side walls. The difference between k and k_0 at any point of the domain will be small by choosing Δ to be small enough except on the solid boundaries, where $k = 0$.

Appendix B: The Boundary Conditions for the Mean Zonal Velocity

The mean zonal velocity U^* , required boundary conditions on the walls, that is, $y = 0, L$. Charney et al. (1981) for an atmospheric zonal channel justified the mean zonal velocity U being constant over the channel but vanish at its boundaries. For an oceanic zonal channel, where the main forcing is a wind stress Marshall (1981) demonstrated that mean zonal velocity on their boundaries vanishes, if wind stress vanishes and if this velocity is zero initially.

Charney et al. (1981) and IZS used this condition, and in their mathematic treatment, they integrated the meridional gradient of U multiplied by the cosine of the meridional coordinate:

$$\int_0^L \frac{\partial U}{\partial y} \cos(\pi y/L) dy. \quad (\text{B1})$$

However, U is not a continuous and differentiable variable over y because it jumps to zero at $y = 0, L$ and $\cos(\pi y/L) = \pm 1$.

If it is assumed (as the previous authors did) that $\frac{\partial U}{\partial y} = 0$ in B1 there is an inconsistency, since

$$\int_0^L \frac{\partial U}{\partial y} \cos(\pi y/L) dy = \int_0^L \frac{\partial}{\partial y} \{\cos(\pi y/L)U\} dy + \pi/L \int_0^L U \sin(\pi y/L) dy. \quad (\text{B2})$$

The first integral on the R.H.S. of B2 equals zero, since U is zero on the walls, but the second integral is not zero. To solve this problem, we suggest to use the following form of U^* :

$$U^* = U \{1 + e^{(-L/\Delta)} - e^{(-y/\Delta)} - e^{(y-L)/\Delta}\}, \quad (\text{B3})$$

where $\Delta \ll L$ and U is a constant. U^* is differentiable on this interval. U^* is almost constant in the domain but quickly drops to zero on the side walls. The difference between U and U^* at any point of the domain will be small by choosing Δ to be small enough, except on the solid boundaries, where $U^* = 0$.

Appendix C: Coefficients k_0 (m²/s) Averaged over Windstress

1. k_0 for topography $C_1 = 100\text{m}$: 505.9
2. k_0 for topography $C_2 = 100\text{m}$: 636.4
3. k_0 for topography $C_3 = 100\text{m}$: 755.2
4. k_0 for topography $C_5 = 100\text{m}$: 460.9
5. k_0 for topography $C_6 = 100\text{m}$: 411.7
6. k_0 for topography $C_7 = 100\text{m}$: 317.5

7. k_0 for topography $C_1 = 200\text{m}$: 777.2
8. k_0 for topography $C_2 = 200\text{m}$: 704.7
9. k_0 for topography $C_3 = 200\text{m}$: 357.2
10. k_0 for topography $C_5 = 200\text{m}$: 267.2
11. k_0 for topography $C_6 = 200\text{m}$: 160.9
12. k_0 for topography $C_7 = 200\text{m}$: 84.1
13. k_0 for topography $C_1 = 300\text{m}$: 722.7
14. k_0 for topography $C_2 = 300\text{m}$: 306.1
15. k_0 for topography $C_3 = 300\text{m}$: 123.5
16. k_0 for topography $C_5 = 300\text{m}$: 50.6
17. k_0 for topography $C_6 = 300\text{m}$: 46.6
18. k_0 for topography $C_7 = 300\text{m}$: 27.2

Appendix D: Developing a Linear Expression Linking k_0 and U

Equation 27 after neglecting of the cubic and the quadratic terms of k_0 and also after neglecting of the 3-rd–5-th terms in (30) can be rewritten as

$$U^3 E_1 + U^2 \sum_{i=2}^4 E_i + U \sum_{i=5}^{13} E_i + \sum_{i=14}^{22} E_i = 0, \quad (\text{D1})$$

where

$$E_1 = 48Hen^2 \pi^2 / L_x, \quad (\text{D2})$$

$$E_2 = -24HL_x \epsilon \beta, \quad (\text{D3})$$

$$E_3 = -12\tau_0 \rho_0^{-1} \pi^3 n^2 / L_x, \quad (\text{D4})$$

$$E_4 = 48k_0 H \beta n^2 \pi^2 / L_x, \quad (\text{D5})$$

$$E_5 = 3HL_x^3 \epsilon \beta^2 / (n^2 \pi^2), \quad (\text{D6})$$

$$E_6 = 12HL_x \epsilon^3, \quad (\text{D7})$$

$$E_7 = 6HL_x^3 \epsilon^3 / (L^2 n^2), \quad (\text{D8})$$

$$E_8 = 3HL_x^5 \epsilon^3 / (4L^4 n^4), \quad (\text{D9})$$

$$E_9 = 6\tau_0 \rho_0^{-1} \pi L_x \beta, \quad (\text{D10})$$

$$E_{10} = 4f_0^2 (c_n^2 + d_n^2) \epsilon L_x / H, \quad (\text{D11})$$

$$E_{11} = f_0^2 (c_n^2 + d_n^2) \epsilon L_x^3 / (Hn^2 L^2), \quad (\text{D12})$$

$$E_{12} = 4k_0 f_0^2 \pi^2 (c_n^2 + d_n^2) L_x / (HL^2), \quad (\text{D13})$$

$$E_{13} = -24k_0 HL_x \beta^2, \quad (\text{D14})$$

$$E_{14} = -3\tau_0 \rho_0^{-1} L_x^3 \beta^2 / (4n^2 \pi), \quad (\text{D15})$$

$$E_{15} = 3\tau_0 \rho_0^{-1} \pi L_x \epsilon^2, \quad (\text{D16})$$

$$E_{16} = -3\tau_0 \rho_0^{-1} \pi \epsilon^2 L_x^3 / (2L^2 n^2), \quad (\text{D17})$$

$$E_{17} = -3\tau_0 \rho_0^{-1} \pi L_x^5 \epsilon^2 / (16L^4 n^4), \quad (\text{D18})$$

$$E_{18} = 4k_0 f_0^2 (c_n^2 + d_n^2) \beta L_x / H, \quad (D19)$$

$$E_{19} = 3k_0 H L_x^3 \beta^3 / (n^2 \pi^2), \quad (D20)$$

$$E_{20} = 12k_0 H L_x \beta \epsilon^2, \quad (D21)$$

$$E_{21} = 6k_0 H L_x^3 \beta \epsilon^2 / (L^2 n^2), \quad (D22)$$

$$E_{22} = 3k_0 H L_x^5 \beta \epsilon^2 / (4L^4 n^4). \quad (D23)$$

The member $|U^3 E_1|$ is much smaller compared with the modulus of all the other terms: usually 3 or 4 orders of magnitude less than the biggest and not higher than 0.03. The term $|U^2 \sum_{i=2}^4 E_i|$ is also smaller than the other terms. Usually, this term is a few percent of the biggest terms. Its contribution is highest for the small amplitude topography ($c_n = 100$ m) but no more than 0.24. For highest accuracy, one can use all the terms without neglecting the smallest or even use the basic cubic equation relative to k_0 (i.e., 27). However for our purposes (linear link between U and k_0) neglecting of terms proportional to U^3 and U^2 is reasonable and Equation D1 can be rewritten as Equation 37.

Appendix E: Additional (Control) Experiments With Random Windstress and Topography

Exp.1: topography $c_3 = 150$ m, $\tau_0 = 0.22$ N/m².

Exp.2: topography $c_5 = 250$ m, $\tau_0 = 0.18$ N/m².

Exp.3: topography $c_2 = 275$ m, $\tau_0 = 0.27$ N/m².

Exp.4: topography $c_1 = 225$ m, $\tau_0 = 0.13$ N/m².

Exp.5: topography $c_6 = 180$ m, $\tau_0 = 0.17$ N/m².

Exp.6: topography $c_4 = 240$ m, $\tau_0 = 0.12$ N/m².

Exp.7: topography $c_7 = 120$ m, $\tau_0 = 0.27$ N/m².

Exp.8: topography $c_2 = 160$ m, $\tau_0 = 0.18$ N/m².

Exp.9: topography $c_3 = 230$ m, $\tau_0 = 0.17$ N/m².

Exp.10: topography $c_1 = 180$ m, $\tau_0 = 0.22$ N/m².

Exp.11: topography $c_2 = 120$ m, $\tau_0 = 0.16$ N/m².

Exp.12: topography $c_4 = 190$ m, $\tau_0 = 0.17$ N/m².

Exp.13: topography $c_5 = 210$ m, $\tau_0 = 0.21$ N/m².

Exp.14: topography $c_1 = 120$ m, $\tau_0 = 0.18$ N/m².

Data Availability Statement

The code and input files required to enable the reader to reproduce the results we present are available online (Sinha and Ivchenko (2022)).

References

- Arakawa, A. (1966). Computational design for long term numerical integration of the equations of fluid motion: Two dimensional incompressible flow. Part 1. *Journal of Computational Physics*, 1, 119–143. [https://doi.org/10.1016/0021-9991\(66\)90015-5](https://doi.org/10.1016/0021-9991(66)90015-5)
- Arakawa, A., & Lamb, V. R. (1977). Computational design of the basic dynamical processes of the UCLA general circulation model. *Methods in Computational Physics*, 17, 173–265. <https://doi.org/10.1016/b978-0-12-460817-7.50009-4>

Acknowledgments

We thank two anonymous reviewers for useful comments and discussion that led to a greatly improved manuscript. VOI acknowledges the support of the University of Southampton and National Oceanography Centre. BS was supported by the UK Natural Environment Research Council CLASS National Capability program.

- Charney, J. G., Shukla, J., & Mo, K. C. (1981). Comparison of a barotropic blocking theory with observation. *Journal of the Atmospheric Sciences*, 38(4), 762–779. [https://doi.org/10.1175/1520-0469\(1981\)038<0762:coabtb>2.0.co;2](https://doi.org/10.1175/1520-0469(1981)038<0762:coabtb>2.0.co;2)
- Constantinou, N. C., & Hogg, A. M. (2019). Eddy saturation of the Southern Ocean: A baroclinic versus barotropic perspective. *Geophysical Research Letters*, 46(21), 12202–12212. <https://doi.org/10.1029/2019gl084117>
- Constantinou, N. C., & Young, W. R. (2017). Beta-plane turbulence above monoscale topography. *Journal of Fluid Mechanics*, 827, 415–447. <https://doi.org/10.1017/jfm.2017.482>
- Cummins, P. F. (2000). Remarks on potential vorticity mixing over topography and momentum conservation. *Deep-Sea Research*, 1(47), 737–743. [https://doi.org/10.1016/s0967-0637\(99\)00107-7](https://doi.org/10.1016/s0967-0637(99)00107-7)
- Dritschel, D., & McIntyre, M. E. (2008). Multiple jets as PV staircases: The Philips effect and the resilience of eddy-transport barriers. *Journal of the Atmospheric Sciences*, 65(3), 855–874. <https://doi.org/10.1175/2007jas2227.1>
- Eden, C. (2010). Parameterising meso-scale eddy momentum fluxes based on potential vorticity mixing and a gauge term. *Ocean Modelling*, 32(1–2), 58–71. <https://doi.org/10.1016/j.ocemod.2009.10.008>
- Eden, C., & Greatbatch, R. J. (2008). Towards a mesoscale eddy closure. *Ocean Modelling*, 20(3), 223–239. <https://doi.org/10.1016/j.ocemod.2007.09.002>
- Fox-Kemper, B., Ferrari, R., & Pedlosky, J. (2003). On the indeterminacy of rotational and divergent eddy fluxes. *Journal of Physical Oceanography*, 33(2), 478–483. [https://doi.org/10.1175/1520-0485\(2003\)033<0478:otiora>2.0.co;2](https://doi.org/10.1175/1520-0485(2003)033<0478:otiora>2.0.co;2)
- Gent, P. B., & McWilliams, J. C. (1990). Isopycnal mixing in ocean circulation models. *Journal of Physical Oceanography*, 20(1), 150–155. [https://doi.org/10.1175/1520-0485\(1990\)020<0150:imiocm>2.0.co;2](https://doi.org/10.1175/1520-0485(1990)020<0150:imiocm>2.0.co;2)
- Green, J. S. A. (1970). Transfer properties of the large-scale eddies and the general circulation of the atmosphere. *Quarterly Journal of the Royal Meteorological Society*, 96(408), 157–185. <https://doi.org/10.1002/qj.49709640802>
- Hallberg, R., & Gnanadesikan, A. (2001). An exploration of the role of transient eddies in determining the transport of a zonally reentrant current. *Journal of Physical Oceanography*, 31(11), 3312–3330. [https://doi.org/10.1175/1520-0485\(2001\)031<3312:aeotro>2.0.co;2](https://doi.org/10.1175/1520-0485(2001)031<3312:aeotro>2.0.co;2)
- Held, I. M. (1975). Momentum transport by quasi-geostrophic eddies. *Journal of the Atmospheric Sciences*, 32(7), 1494–1497. [https://doi.org/10.1175/1520-0469\(1975\)032<1494:mtbqge>2.0.co;2](https://doi.org/10.1175/1520-0469(1975)032<1494:mtbqge>2.0.co;2)
- Ivchenko, V. O. (1984). Parameterization of the eddy fluxes of the quasi-geostrophic potential vorticity in zonal flows. *Doklady Akademii Nauk USSR*, 277, 972–976.
- Ivchenko, V. O., Danilov, S., & Schroeter, J. (2014b). Comparison of the effect of parameterized eddy fluxes of thickness and potential vorticity. *Journal of Physical Oceanography*, 44, 2470–2484. <https://doi.org/10.1175/JPO-D-13-0267.1>
- Ivchenko, V. O., Danilov, S., Sinha, B., & Schroeder, J. (2014a). Integral constraints for momentum and energy in zonal flows with parameterized potential vorticity fluxes: Governing parameters. *Journal of Physical Oceanography*, 44(3), 922–943. <https://doi.org/10.1175/JPO-D-13-0173.1>
- Ivchenko, V. O., Richards, K. J., Sinha, B., & Wolff, J.-O. (1997). Parameterization of mesoscale eddy fluxes in zonal ocean flows. *Journal of Marine Research*, 55(6), 1127–1162. <https://doi.org/10.1357/0022240973224076>
- Ivchenko, V. O., Sinha, B., Zalesny, V. B., Marsh, R., & Blaker, A. T. (2013). Influence of bottom topography on integral constraints in zonal flows with parameterized potential vorticity fluxes. *Journal of Physical Oceanography*, 43(2), 311–323. <https://doi.org/10.1175/jpo-d-12-0126.1>
- Ivchenko, V. O., Richards, K. J., & Stevens, D. P. (1996). The dynamics of the antarctic circumpolar current. *Journal of Physical Oceanography*, 26(5), 753–774. [https://doi.org/10.1175/1520-0485\(1996\)026<0753:tdotac>2.0.co;2](https://doi.org/10.1175/1520-0485(1996)026<0753:tdotac>2.0.co;2)
- Ivchenko, V. O., Zalesny, V. B., & Sinha, B. (2018). Is the coefficient of eddy potential vorticity diffusion positive? Part 1: Barotropic zonal flow. *Journal of Physical Oceanography*, 48(7), 1589–1607. <https://doi.org/10.1175/jpo-d-17-0229.1>
- Johnson, G. C., & Bryden, H. (1989). On the size of the antarctic circumpolar current. *Deep-Sea Research*, 36(1), 39–53. [https://doi.org/10.1016/0198-0149\(89\)90017-4](https://doi.org/10.1016/0198-0149(89)90017-4)
- Killworth, P. D. (1997). On the parameterization of eddy transfer. Part 1. Theory. *Journal of Marine Research*, 55(6), 1171–1197. <https://doi.org/10.1357/0022240973224102>
- Marshall, D. P., & Adcroft, A. J. (2010). Parameterization of ocean eddies: Potential vorticity mixing, energetics and Arnold’s first stability theorem. *Ocean Modelling*, 32(3–4), 188–204. <https://doi.org/10.1016/j.ocemod.2010.02.001>
- Marshall, D. P., Maddison, J. R., & Berloff, P. S. (2012). A framework for parameterizing eddy potential vorticity fluxes. *Journal of Physical Oceanography*, 42(4), 539–557. <https://doi.org/10.1175/jpo-d-11-048.1>
- Marshall, J. C. (1981). On the parameterization of geostrophic eddies in the ocean. *Journal of Physical Oceanography*, 11(2), 257–271. [https://doi.org/10.1175/1520-0485\(1981\)011<0257:otpoge>2.0.co;2](https://doi.org/10.1175/1520-0485(1981)011<0257:otpoge>2.0.co;2)
- Marshall, J. C., Olbers, D., Ross, H., & Wolff-Gladrow, D. (1993). Potential vorticity constraints on the dynamics and hydrography of the Southern Ocean. *Journal of Physical Oceanography*, 23(3), 465–487. [https://doi.org/10.1175/1520-0485\(1993\)023<0465:pvcotd>2.0.co;2](https://doi.org/10.1175/1520-0485(1993)023<0465:pvcotd>2.0.co;2)
- McWilliams, J. C., Holland, W. R., & Chow, J. S. (1978). A description of numerical antarctic circumpolar currents. *Dynamics of Atmospheres and Oceans*, 2(3), 213–291. [https://doi.org/10.1016/0377-0265\(78\)90018-0](https://doi.org/10.1016/0377-0265(78)90018-0)
- Munday, D. R., Johnson, H. L., & Marshall, D. P. (2013). Eddy saturation of equilibrated circumpolar currents. *Journal of Physical Oceanography*, 43(3), 507–532. <https://doi.org/10.1175/jpo-d-12-095.1>
- Munk, W. H., & Palmén, E. (1951). Note on the dynamics of the antarctic circumpolar current. *Tellus*, 3(1), 53–55. <https://doi.org/10.3402/tellusa.v3i1.8609>
- Olbers, D., Wolff, J.-O., & Voelker, C. (2000). Eddy fluxes and second-order moment balances for nonhomogeneous quasigeostrophic turbulence in wind-driven zonal flows. *Journal of Physical Oceanography*, 30(7), 1645–1668. [https://doi.org/10.1175/1520-0485\(2000\)030<1645:efasom>2.0.co;2](https://doi.org/10.1175/1520-0485(2000)030<1645:efasom>2.0.co;2)
- Richtmyer, R. D., & Morton, K. W. (1967). *Difference Methods for Initial-Value Problems* (2d ed.). J. Wiley and Sons.
- Ringler, T., & Gent, P. (2011). An eddy closure for potential vorticity. *Ocean Modelling*, 39(1–2), 125–134. <https://doi.org/10.1016/j.ocemod.2011.02.003>
- Sinha, B., & Ivchenko, V. O. (2022). NOC-MSM/PVdiffusion (version 1.0) [Dataset]. *Zenodo*. <https://doi.org/10.5281/zenodo.6563283>
- Sinha, B., & Richards, K. J. (1999). Jet structure and scaling in Southern Ocean models. *Journal of Physical Oceanography*, 29(6), 1143–1155. [https://doi.org/10.1175/1520-0485\(1999\)029<1143:jsasis>2.0.co;2](https://doi.org/10.1175/1520-0485(1999)029<1143:jsasis>2.0.co;2)
- Stevens, D. P., & Ivchenko, V. O. (1997). The zonal momentum balance in an eddy-resolving general-circulation model of the Southern Ocean. *Quarterly Journal of the Royal Meteorological Society*, 123(540), 929–951. <https://doi.org/10.1002/qj.49712354008>
- Tansley, C. E., & Marshall, D. P. (2001). On the dynamics of wind-driven circumpolar currents. *Journal of Physical Oceanography*, 31(11), 3258–3273. [https://doi.org/10.1175/1520-0485\(2001\)031<3258:otdowd>2.0.co;2](https://doi.org/10.1175/1520-0485(2001)031<3258:otdowd>2.0.co;2)

- Treguier, A. M., Held, I. M., & Larichev, V. D. (1997). Parameterization of quasigeostrophic eddies in primitive equation ocean models. *Journal of Physical Oceanography*, 27(4), 567–580. [https://doi.org/10.1175/1520-0485\(1997\)027<0567:poeip>2.0.co;2](https://doi.org/10.1175/1520-0485(1997)027<0567:poeip>2.0.co;2)
- Treguier, A. M., & McWilliams, J. C. (1990). Topographic influences on wind-driven, stratified flow in a β -plane channel. *Journal of Physical Oceanography*, 20(3), 321–343. [https://doi.org/10.1175/1520-0485\(1990\)020<0321:tiowds>2.0.co;2](https://doi.org/10.1175/1520-0485(1990)020<0321:tiowds>2.0.co;2)
- Wardle, R., & Marshall, J. (2000). Representation of eddies in primitive equation models by a PV flux. *Journal of Physical Oceanography*, 30(10), 2481–2503. [https://doi.org/10.1175/1520-0485\(2000\)030<2481:roeipe>2.0.co;2](https://doi.org/10.1175/1520-0485(2000)030<2481:roeipe>2.0.co;2)
- Welander, P. (1973). Lateral friction in the ocean as an effect of potential vorticity mixing. *Geophysical Fluid Dynamics*, 5(1), 173–189. <https://doi.org/10.1080/03091927308236114>
- Wolff, J.-O., Maier-Reimer, E., & Olbers, D. (1991). Wind-driven flow over topography in a zonal β -plane channel: A quasigeostrophic model of the antarctic circumpolar current. *Journal of Physical Oceanography*, 21(2), 236–264. [https://doi.org/10.1175/1520-0485\(1991\)021<0236:wdfoti>2.0.co;2](https://doi.org/10.1175/1520-0485(1991)021<0236:wdfoti>2.0.co;2)
- Wood, R. B., & McIntyre, M. E. (2010). A general theorem on angular-momentum changes due to potential vorticity mixing and on potential-energy changes due to buoyancy mixing. *Journal of the Atmospheric Sciences*, 67(4), 1261–1274. <https://doi.org/10.1175/2009jas3293.1>
- Wunsch, C. (2003). Determining palaeoceanography circulations, with emphasis on the last glacial maximum. *Quaternary Science Reviews*, 22(2–4), 371–385. [https://doi.org/10.1016/s0277-3791\(02\)00177-4](https://doi.org/10.1016/s0277-3791(02)00177-4)